Journal of Colloid and Interface Science 536 (2019) 372–380

Contents lists available at ScienceDirect

Journal of Colloid and Interface Science

journal homepage: www.elsevier.com/locate/jcis

Regular Article

Smart release of antimicrobial ZnO nanoplates from a pH-responsive keratin hydrogel

María E. Villanueva [a,b], María L. Cuestas [c], Claudio J. Pérez [d], Viviana Campo Dall′ Orto [a,b], Guillermo J. Copello [a,b,*]

[a] Universidad de Buenos Aires (UBA), Facultad de Farmacia y Bioquímica, Departamento de Química Analítica y Fisicoquímica, (UBA), Junín 956, C1113AAD Buenos Aires, Argentina
[b] Instituto de Química y Metabolismo del Fármaco, Fac. de Farmacia y Bioquímica, (IQUIMEFA-UBA-CONICET), Argentina
[c] Instituto de Investigaciones en Microbiología y Parasitología Médica (IMPaM), CONICET-Universidad de Buenos Aires, Paraguay 2155, C1121ABG piso 11, Buenos Aires, Argentina
[d] Grupo Ciencia e Ingeniería de Polímeros, Instituto en Investigaciones en Ciencia y Tecnología de Materiales, Universidad de Mar del Plata, (CONICET), Juan B. Justo 4302, CP7600 Mar del Plata, Argentina

GRAPHICAL ABSTRACT

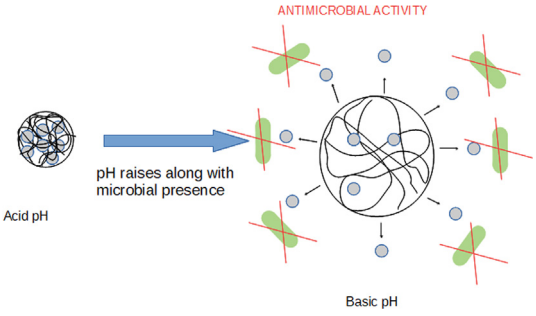

ARTICLE INFO

Article history:
Received 8 August 2018
Revised 19 October 2018
Accepted 22 October 2018
Available online 24 October 2018

Keywords:
Zinc oxide nanoparticles
Smart keratin hydrogels
Antimicrobial wound dressings
Biodegradable
Biocompatible

ABSTRACT

A smart antibacterial biomaterial based on a keratin hydrogel with pH-dependent behavior and Zinc Oxide nanoplates as biocide agent has been developed. The pH of a chronic wound is basic due to bacterial metabolism. Originally shrank at acid pH, keratin hydrogels swell upon contact with a bacterial contaminated media leading to the release of the nanoparticles. The material has been thoroughly characterized by infrared spectroscopy, Raman, scanning electron microscope, swelling behavior, Differential scanning calorimetry, Small-angle X-ray scattering, rheology, antimicrobial activity and cytotoxicity. The results show that 5% of Zinc Oxide nanoparticles concentration is the optimum for wound dressing applications.

1. Introduction

The infection of a wound is one of the main concerns regarding its cure [1]. Infection usually occurs due to the interaction between the microorganisms with the wound and the used dressings [2–4], preventing wound healing. Historically, wound treatment has evolved with mankind civilization. Many years ago, the wound was only covered to protect the area and absorb the exudates. Nowadays, different types of dressings are used to maintain moisture, prevent infection and promote healing [5]. There are many types of dressings: fibers, sponges, membranes, etc. Dressings

* Corresponding author at: Junin 956, PC: C1113AAD Buenos Aires, Argentina.
E-mail address: gcopello@ffyb.uba.ar (G.J. Copello).

https://doi.org/10.1016/j.jcis.2018.10.067
0021-9797/

may be made from synthetic or natural materials. Recently, hydrogels have also been used since they can swell in a liquid medium and maintain a humid environment, avoiding dehydration of the wound. The generated wet environment provides optimum conditions to reduce pain, promote cell mobility and maintain hydration and tissue structure [6,7].

Keratin is a low cost and highly available precursor for hydrogels development [8,9]. It can be obtained from waste materials from the livestock and poultry industry, such as hair, wool, hooves, horns, feathers, and also, from a human source. Due to the characteristics of the material, porous sponge-like structures or flexible films can be obtained [10,11]. In a previous work, a pH-responsive keratin hydrogel was obtained by a partial hydrolysis method. Two extreme states were detected. One at low pH, for which swelling is minimum, and one at high pH, for which swelling is maximum. In addition, the material responsiveness was reversible [12].

The incorporation of nanoparticulate materials into different matrices has attracted attention because it has demonstrated the capacity to reinforce the structure of biomaterials [13,14] and may add other characteristics such as antimicrobial power [15,16]. In this sense, the study of the incorporation of nanoparticles presents a promising alternative for obtaining nanocomposites to be used as dressings [17–19].

ZnO nanoparticles (nZnO) have shown to possess great antibacterial activity without generating adverse effects on eukaryotic cells [20]. The enhanced bactericidal effect of nZnO compared to Zinc salts has been attributed to their small size and high surface to volume ratio, which allow them to interact closely with microbial membranes. Besides, their antimicrobial activity is not merely due to the release of metal ions in solution but also to the generation of reactive oxygen species with subsequent oxidative damage to cellular structures [21,22]. Moreover, the Zinc ions released from the nanoparticles promote the migration of keratinocytes to the wound, favoring the healing [23–25]. In recent years, several developments have been performed in which hydrogels are combined with ZnO nanoparticles to be used as dressings [16,18,25,26].

In this work, a smart material was developed and characterized, in order to establish its potential use as an antimicrobial wound dressing, an application of high relevance for the medical products industry. Three nanocomposites were obtained and named according to the nZnO concentration: 1% nZnO Ker hydrogel, 5% nZnO Ker hydrogel and 10% nZnO Ker hydrogel. This smart material responded to changes in the pH of the medium. At basic pH, the gel matrix is expanded increasing the swelling and at acid pH, is collapsed, decreasing it. The pH of a chronic wound is basic because of the products of bacterial metabolism and as the wound heals, the pH becomes more acidic [27,28]. In this way, when the bacterial contamination is low, the pH of the medium will be lower, leading to a lower swelling of the gel, a smaller pore size and the lesser release of the nZnO. With the pH change occurring as a consequence of bacterial contamination, the keratin hydrogel will swell, the pore size will increase and the release of the nanoparticulate biocidal agent will occur to a greater extent.

2. Materials and methods

2.1. Materials

The bovine horn was kindly provided by Veterinarian Juan Fernandez Pego, Zinc Sulfate ($ZnSO_4$. 7 H_2O, 99.8%) was purchased from Mallinckrodt (New York, USA) and urea was purchased from Biopack (99.8%, Buenos Aires, Argentina). The bacterium *Staphylococcus aureus* ATCC 29213 was kindly provided by the Microbial Culture Collection of the Faculty of Pharmacy and Biochemistry (CCM 29) and the bacterium *Escherichia coli* wild type was isolated from a hospital environment. Dulbecco's modified Eagle's medium (DMEM) and fetal bovine serum (FBS) were purchased from Life Technologies Corp. (Carlsbad, USA). The other reagents used were of analytical grade.

2.2. Synthesis of zinc oxide nanoplates

Zinc sulfate was mixed with urea to total dissolution, concentrations of Zn^{2+} and urea in the solutions were adjusted to 2.4 and 3.3 mM, respectively. Then a solution of 3 M NaOH was added drop-wise until a whitish suspension was obtained. The product was washed with water 3 times by centrifugation and resuspension. The yield of the synthesis was 77.5%.

2.3. Hydrogel synthesis

Horn was milled and sieved through a 250 μm sieve. Then, the horn powder was washed three times with distilled water and with ethyl acetate to remove fat. After that, the powder was dried at 37 °C overnight. Keratin (1 g) powder was mixed with 7 ml dilution of 1 N NaOH in Ethanol (25 ml). The mixture was left at 45 °C for 4 h. After that, it was mixed with different amounts of nZnO (in order to obtain a 1, 5 and 10% w/w nZnO Ker hydrogels), the mixtures were homogenized through a syringe and left until complete dryness at 45 °C. The final product was a dry block of keratin that was easily hydrated in water to form the hydrogel. The keratin blocks obtained, were thoroughly washed with deionized water in order to remove all NaOH residue. After hydration, the hydrogel form of the material was obtained.

2.4. Characterization

2.4.1. Spectroscopic characterization

ATR-FTIR (diamond attenuated total reflectance) of keratin materials were recorded using a Nicolet iS50 Advanced Spectrometer (Thermo Scientific). ATR-FTIR spectra were recorded with 32 scans and a resolution of 4 cm^{-1}. FT-Raman spectra were acquired with an excitation laser beam of 1064 nm, 0.5 W laser power, resolution of 4 cm^{-1}, 50 scans. All samples were previously dried for 24 h at 60 °C to avoid water related bands interference.

2.4.2. Swelling behavior

In order to assess the swelling behavior of the material, 0.02 g of a keratin block were equilibrated in different 10 mM phosphate solutions ranging from pH 4 to pH 8. After equilibrium was reached, the hydrogels were removed from the solution and accurately weighted.

2.4.3. Scanning electron microscopy (SEM)

Electron microscopy images were obtained on a Zeiss Supra 40 and Quanta FEG 250 scanning electron microscopes. The hydrogels were dried and coated with gold, before the observation.

2.4.4. Rheological behavior

The rheological behavior of the hydrogels with different nZnO content was studied. Amplitude sweeps were performed first in order to determine the linear viscoelastic range (LVR). The elastic or storage modulus, G' (ω), the viscous or loss modulus, G'' (ω) and complex viscosity (η^*) of the studied materials were obtained in small-amplitude oscillatory shear flow experiments using a rotational rheometer from Anton Paar (MCR-301) provided with a CTD 600 thermo chamber. The tests were performed using parallel plates of 25 mm diameter and a frequency range of 0.1–500 s^{-1}. The measurements were carried out at room temperature (20 °C). All the tests were performed using small strains ($\gamma = 0.5\%$) to

ensure the linearity of the dynamic responses. All the runs were repeated using different samples. The gap width used was 700–800 μm.

2.4.5. Small angle X-ray scattering (SAXS)

SAXS experiments were performed at INIFTA (La Plata, Argentina, project "Nanopymes", EuropeAid/132184/D/SUP/AR-Contract 331-896) facilities using a XEUSS 1.0 equipment from XENOCS with a Kα-Cu radiation microsource (λ = 0.154 nm). A PILATUS-100 K detector (DECTRIS AG, Switzerland) was used in two sample to detector distances, 530 mm and 2495 mm. An exposure time of 600 s was used. The samples were placed with their surfaces perpendicular to the direction of the incident X-ray beam and parallel to the X-ray detector. The scattering intensity (I) was measured as a function of the scattering vector (q) from 0.004 to 0.66 $Å^{-1}$. The background and parasitic scattering were determined by using an empty sample holder and were subtracted for each measurement.

2.4.6. Differential scanning calorimetry (DSC, thermal analysis)

Differential scanning calorimetry was performed using a Shimadzu DSC-50 device. Freeze-dried samples were tested from 20 °C to 260 °C at a heating rate of 10 °C/min, under nitrogen flow.

2.5. Zinc quantification.

The total Zinc concentration in the hydrogels was determined by treating the samples (10–20 mg) with nitric acid and hydrogen peroxide (9:1) (1 ml). To determine the release of Zn under different pH conditions, an agar suspension was prepared in solutions at pH 4 and 8. They were heated until complete dissolution was achieved. Then disks of 1.5 cm in diameter and 1 ml in volume were assembled. Disks of the keratin hydrogel with and without nanoplates were supported on these discs and left in contact for 18 h. After that time, the release of Zn to the agar-agar gel was evaluated by mineralization as described above and determined by Atomic Absorption Spectroscopy using a Perkin Elmer Analyst 200.

2.6. Antimicrobial effectiveness tests.

The minimum inhibitory concentration was performed by microdilution according to the standards of the Clinical and Laboratory Standards Institute (CLSI) [38]. The nZnO were tested at the concentrations of 3.1–31.2 μg mL^{-1} against *E. coli.* The microplates were incubated for 24 h at 35° C and then counted by the spread plate method.

The antibacterial activity of the hydrogels against *E. coli* and *S. aureus* was performed according to a modified assay from Japanese Industrial Standards (JIS) Z 2801 [29]. For this test microorganisms were grown in LB medium for 24 h. The challenge inoculum was prepared diluting the grown bacteria with a culture medium (LB medium diluted 500-fold in physiological sterile solution) until the microorganism concentration was 5.3 10^6 cfu/mL for *E. coli* and 4.0 10^6 cfu/mL for *S. aureus*.

The samples (0.5 cm diameter disks) were disinfected with 1 ml of 70% ethanol and used for the antibacterial efficacy assay after washing three times with sterilized water. Then, they were incubated placing 20 μl of the previously prepared bacterial suspensions on the upper side of the disc at 37 °C. The assay was performed in a chamber in which a container with sterile distilled water was placed to maintain humidity.

After 24 h, the surviving bacteria on the supernatants were counted by the spread plate method. For this purpose, decimal dilutions were spread on a Petri dish that contained LB agar and were incubated at 35 °C for 24 h [30].

The results were presented in terms of value of antibacterial activity (R(log); Eq. (1)) and % bacterial reduction (D%; Eq. (2)).

$$R(\log) = [\log(A) - \log(B)] \quad (1)$$

$$D\% = (A - B)/B \times 100 \quad (2)$$

where A is the average of the number of viable cells of bacteria on the control hydrogel sample after 24 h and B is the average of the number of viable cells of bacteria on the hydrogels loaded with nZnO after 24 h.

A diffusion assay was also performed on LB agar to confirm antibacterial activity [31]. These tests were performed against *E. coli* and *S. aureus* as models pathogens of Gram negative and Gram positive bacteria, respectively to incubate for 24 h at 37° C. In this method, an LB agar plate enriched with the vital dye triphenyl tetrazolium chloride was inoculated with a bacterial suspension adjusted to 10^5 cfu/ml. The hydrogels were then rested on the inoculated medium and after incubation at 37° C for 24 h, the zone of inhibition was observed.

All experiments were performed in triplicate, each time using a fresh cell culture. It was verified that the conditioning procedure of the sample do not alter its swelling behavior.

2.7. Cytotoxicity

2.7.1. Cells and culture conditions

The mammalian continuous cell line derived from the kidney of an African green monkey, Vero cells, were purchased from ATCC (ATCC No: CCL-81). Cells were cultured in Dulbecco's modified Eagle's medium (DMEM) supplemented with 10% fetal bovine serum (FBS) and maintained at 37 °C in a humidified atmosphere of 5% CO_2.

2.7.2. Cytotoxicity assays

Cells were seeded in 12-well plates (1.0×10^6 cells/well), grown overnight and the cytotoxic activity of the hydrogels at different concentrations (1%, 5% and 10%) was determined after 24 h of incubation using the trypan blue exclusion assay according to the UNE-EN ISO 10993-5: 2009 standard [32] which describes the methods that allow to evaluate the *in vitro* cytotoxicity of medical devices. In this assay, two different methods of incubation were carried out: (i) by direct contact of the hydrogels with the cell monolayer and (ii) by adding the hydrogel extracts obtained by elution to the culture medium.

In the first case, after incubating the hydrogels to UV to ensure their sterility, samples were cut with a sterile scalpel so that they were the appropriate size (0.4 cm^2) to cover one tenth of the cell monolayer. In the second case, after incubating the hydrogels with physiological solution for 24 h at 37 °C the resulting extracts were sterilized with 0.22 μm filters and added to the cell cultures. In all cases, 5% DMSO was used as a positive control for cytotoxicity. Untreated cells were used as negative control. These assays were performed in triplicates. It was verified that the conditioning procedure of the sample do not alter its swelling behavior.

2.8. Statistics

All quantitative results were obtained from triplicate samples. Data were expressed as means ± SD. Statistical analysis was carried out using a One-way ANOVA test and a Bonferroni post-test, except where it was indicated otherwise. A value of $p < 0.05$ was considered to be statistically significant.

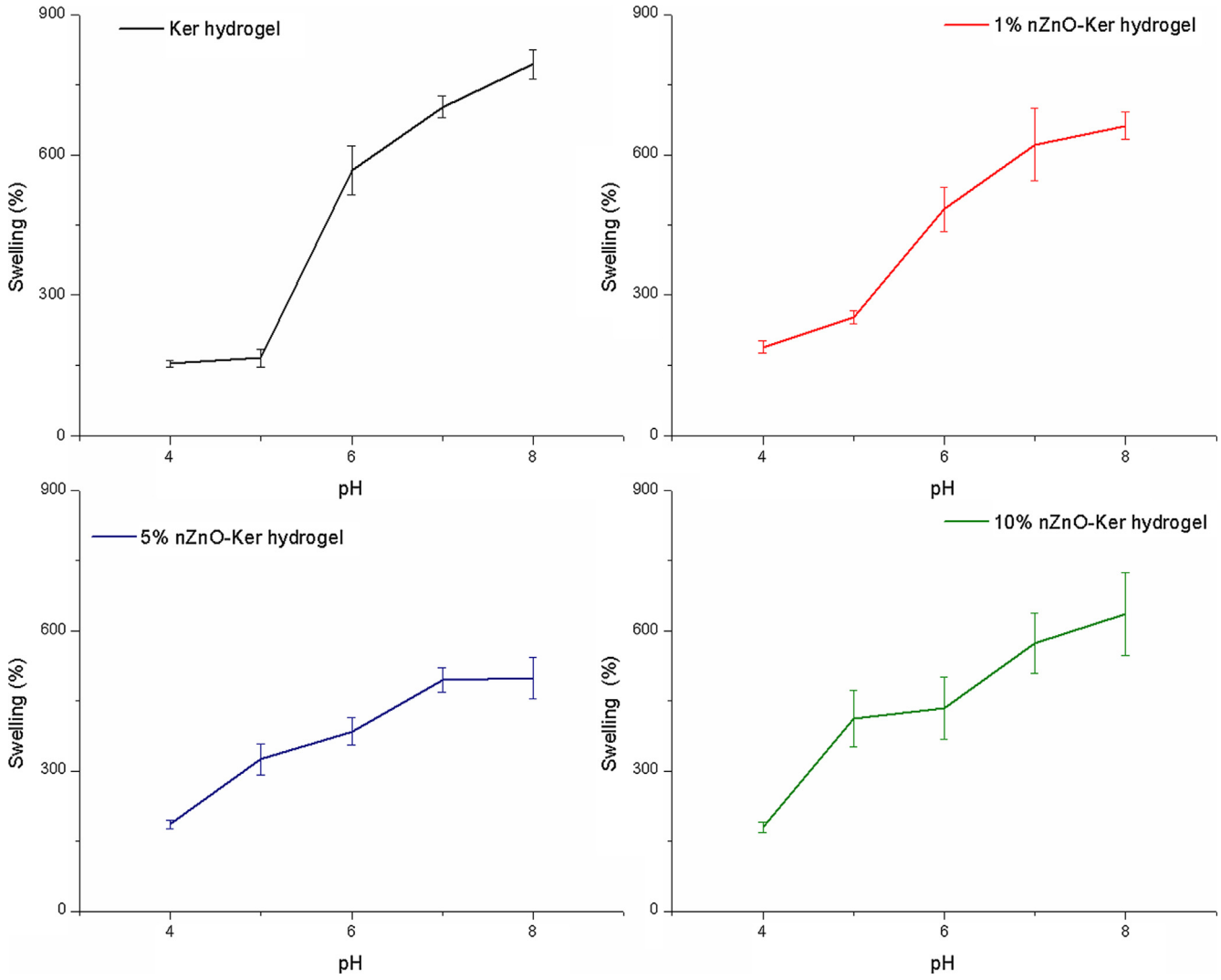

Fig. 1. Swelling behavior of the different Ker hydrogels (±SD, n = 3).

3. Results and discussion

3.1. Spectroscopic characterization

Fig. S1 (Supporting Information) shows the FT-IR spectra of the hydrogels and the nZnO. In the nZnO spectrum the typical bands could be observed. The bands between 600 and 400 cm^{-1} were present due to the Zn—O stretching. In the nanoplates synthesis, the Zn^{2+} reacted with the urea. Firstly, $Zn_4CO_3(OH)_6{\cdot}H_2O$ is formed. That specie was slowly oxidized to form ZnO. The band present at 3280 cm^{-1} corresponded with the O—H stretching of the water molecules [33]. The other bands (959, 1025 and 1123 cm^{-1}) corresponded to remains of the carbonate formed during the nZnO formation [34]. It could be concluded that in the ZnO nanoplates, ZnO as well as $Zn_4CO_3(OH)_6{\cdot}H_2O$ were present.

In the hydrogel spectra keratin characteristic bands could be found: peaks were observed at 1638 cm^{-1}, which corresponded to the vibration of the C=O bond, and at 1535 cm^{-1}, which corresponded to a combination of the C—N stretching and N—H deformation vibrations [35,36]. The strong peaks at around 1100 cm^{-1} could be assigned to SO_4^{2-} groups [37]. The lack of ZnO related bands may be due to the low concentration.

Fig. S2 (Supporting Information) showed the FT-Raman spectra of the nZnO and the different keratin hydrogels. In the nZnO spectrum, the characteristic peaks could be found. The peak at 394 cm^{-1} corresponded to the E_2 high- E_2 low (multi-phonon process), the peak at 447 cm^{-1} corresponded to the A_1 phonon mode

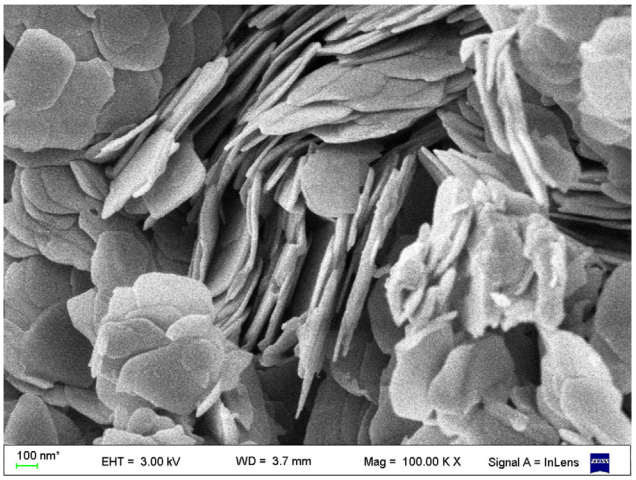

Fig. 2. SEM image of the nZnO.

and the peak at 611 cm^{-1} corresponded to the E_2 high phonon mode. The peak at 986 cm^{-1} corresponded to the optical overtone [38–40].

The FT-Raman spectra of the different hydrogels showed the characteristic bands of the keratin: the band at 1315 and at 1448 cm^{-1} corresponded to C—H and CH_2—CH_3 bending modes respectively. The band at 1606 and 1664 cm^{-1} corresponded to the presence of amide II and I respectively. The bands at 2941 and 3385 cm^{-1} corresponded to CH_3 asymmetric stretching and O—H stretching respectively [41]. The presence of nZnO in the hydrogels could not be evidenced by this method probably due to its low concentration. Nevertheless, these spectroscopic assays showed that no covalent bonds or other types of strong interaction as the ionic interaction were formed.

3.2. Macroscopic characterization and water absorption.

The dried keratin blocks had a rigid structure which swelled upon contact with water forming a hydrogel. The nZnO keratin hydrogels were rigid and compressible and could be handled easily. A pH-dependent behavior of the medium was observed by equilibrating the obtained gels between pH 4 and 8 (Fig. S3, Supporting Information).

The swelling behavior of the different hydrogels was studied by stabilizing them in media with different pH values. As it is shown in Fig. 1, in all cases the swelling behavior of hydrogels increased when the pH values rose ($p < 0.001$). However, the swelling transition points and the swelling % depended on the presence of nZnO. In the Ker and the 1% nZnO hydrogels the swelling transition

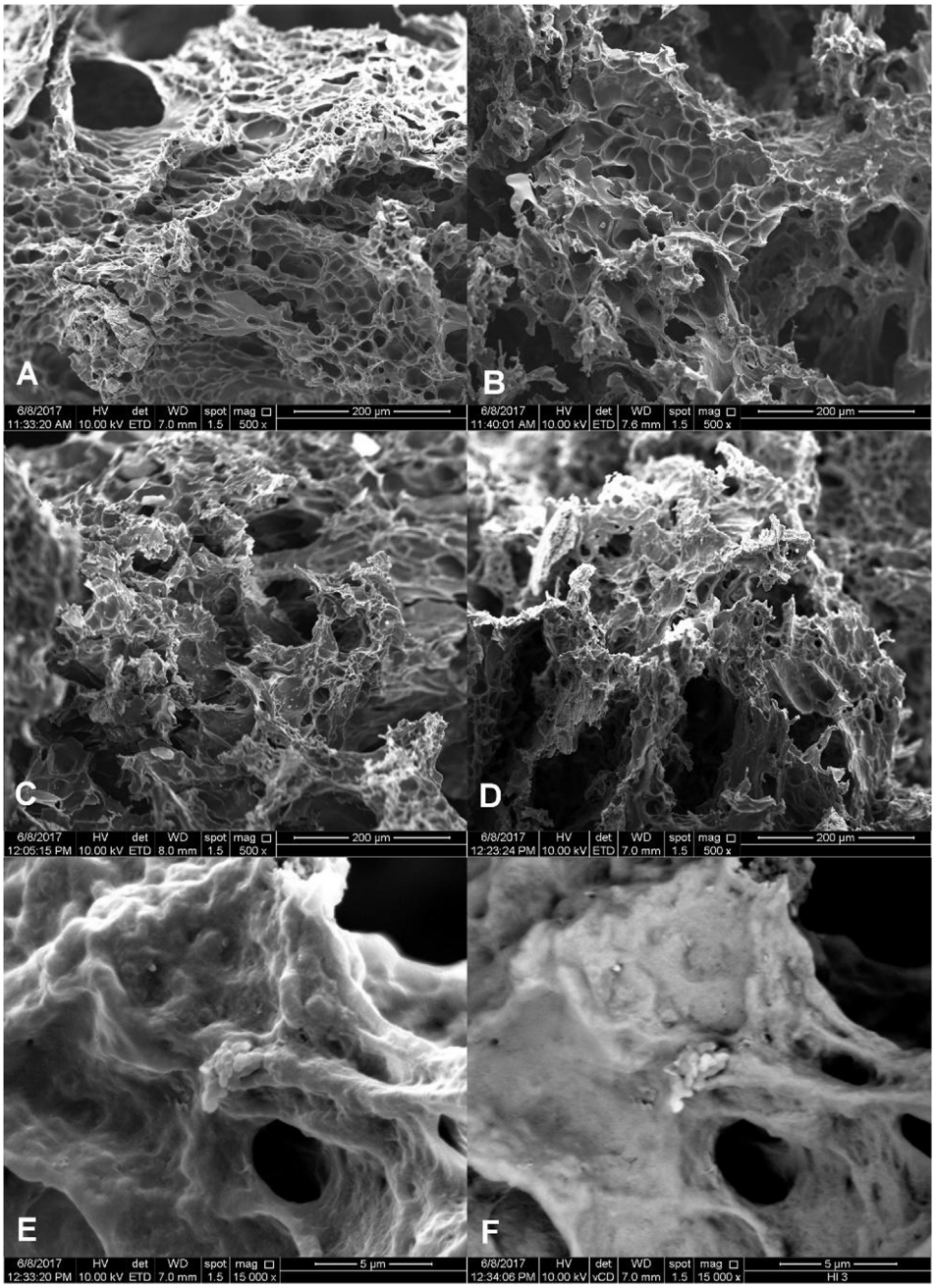

Fig. 3. SEM images of Ker hydrogel (A), 1% nZnO Ker hydrogel (B), 5% nZnO Ker hydrogel (C), 10% nZnO Ker hydrogel (D), nZnO in 10% nZnO Ker hydrogel with Secondary Electron detector (E) and with Backscattered Electron detector (F).

occurred between pH 5 and 6 (they are significantly different $p < 0.001$). The swelling values at pH 7 and 8 were significantly higher than those achieved at pH 6 ($p < 0.05$) and the difference between pH 7 and 8 was not significant ($p > 0.05$). In 5% nZnO Ker and 10% nZnO ker hydrogels, no abrupt change could be observed between the swelling behavior at the subsequent pH values ($p > 0.05$). Besides the % swelling was lower in these hydrogels. The different behavior can be interpreted in terms of the steric hindrance of the keratin chains due to the presence of nZnO. Besides, a certain percentage of the weight corresponded to the nZnO mass, which did not contribute to the swelling.

3.3. Microscopic characterization of Zinc Oxide nanoparticles and hydrogels.

The nanoparticles were observed by scanning electron microscopy. It was observed a nanoplate like structure with polydisperse nanoscale dimensions (Fig. 2). The nanoobjects diameter size was 342.0 ± 69.2 nm and their thickness were 31.1 ± 8.8 nm.

In order to study the microscopic topography of the hydrogels, SEM analysis was carried out (Fig. 3). In a previous work [12], it has been observed that the Ker at low pH values had a collapsed structure and, at higher values of pH, the network was expanded. The observed samples had been equilibrated at pH 7, and a similar structure to the ones observed in the work cited above. The presence of the nanoplates was verified in the nanocomposites by switching to a Backscattered detector. In these images the elements with higher Z were observed with a higher intensity. As could be seen in the Fig. 3F the intensity of the nanoplates is higher than in Fig. 3E. In the 10% nZnO hydrogel the nZnO were distributed heterogeneously and agglomeration was observed.

3.4. Small angle X-ray scattering (SAXS)

The study of the keratin chain organization together with the nZnO was studied at the nanoscale level by means of SAXS. As it can be seen in Fig. 4, the nZnO profile showed three correlation peaks probably due to ZnO nanoplates long periods, that in accordance to the Bragg's law ($d = 2\pi/q$) represented a distance of 12.62 Å, 11.89 Å and 10.61 Å. These peaks were not evidenced in the 1% and 5% nZnO Ker profiles suggesting that the nanoplates were well dispersed within the protein matrix, or not detected. The 10% nZnO Ker profile presented the major peak indicating the presence of agglomerates of the nanoplates as shown by SEM. In the Ker SAXS log-log plot (Fig. 4a) a short regime with lower slope that accounts for the local organization keratin chains was observed. According to the relation $I(q) \sim q^{-\alpha}$, an α value of 1.2 in the q range of 0.02–0.06 $Å^{-1}$ was shown. α values near 1 might account for rod-like structure [42]. This regime was lost in the profiles of the nZnO containing hydrogels. In Fig. 4b, the Kratky representation, used for evidencing the folding state of proteins, highlighted the conformational changes induced on the keratin structure by the presence of increasing concentrations of nZnO in the hydrogels.

3.5. Rheology

Fig. 5 shows the rheological behavior of the hydrogels. The storage modulus (G') was higher than the loss modulus (G'') in all the samples, meaning that the elastic behavior of the material was predominant over the viscous component, a typical characteristic of a gel-like material [43]. The viscoelastic properties of the gels strongly depend on the nZnO concentrations. From SAXS results, it was expected that the changes in the keratin structural organization might impact on the mechanical properties of the hydrogels. As long as nZnO concentration increased, $\acute{G}$ was higher, demonstrating that the addition of the nanoobject reinforced the material. However, this behavior was not observed in the 10% nZnO Ker hydrogel, where $\acute{G}$ was lower than in treated and untreated samples. This result suggested structural heterogeneity at high nZnO concentrations [44].

Fig. 5 also shows the complex viscosity of the gels according to the frequency. In all the samples, the complex viscosity decreased linearly with the rise of frequency, which implied a shear thinning behavior in which the material becomes more fluid as the applied frequency increases. Complex viscosity was lower in the 10% nZnO gel, this was caused by the structural inhomogeneity at high nZnO concentrations.

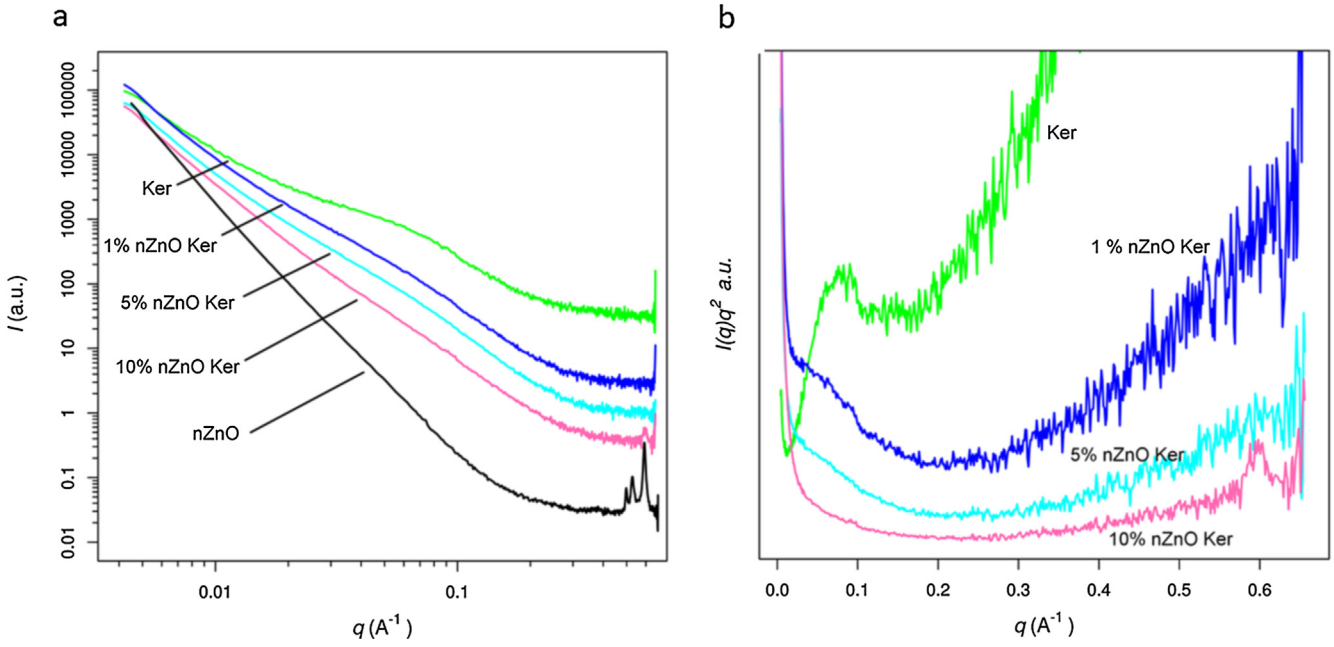

Fig. 4. SAXS profiles of the Ker and the nZnO Ker nanocomposites. Log-log (a) and Kratky representation (b).

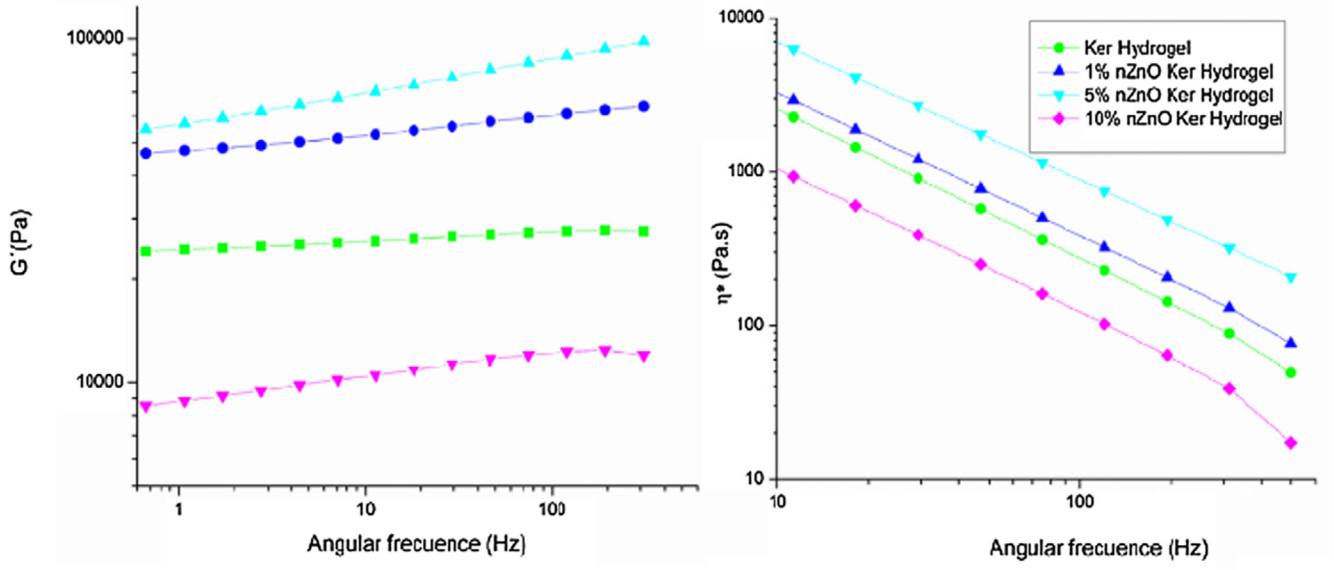

Fig. 5. Storage modulus ($\acute{G}$) and complex viscosity (η^*) frequency dependence of the Ker hydrogel and the nZnO Ker nanocomposites.

3.6. Differential scanning calorimetry (DSC, thermal analysis)

The thermal behavior of the keratin hydrogel and the nanocomposites was studied by DSC, as shown in Fig. 6. Two endothermic events were observed in the thermograms of all samples. The first event, accounted for the desorption of the adsorbed moisture in keratin samples (*Td*). The second event, near 230 °C, accounted for the denaturation of the more crystalline structure of the protein (*Tm*) [45]. From SAXS and Rheological assays it could be expected that the *Tm* peak might vary among samples. Nevertheless, since in this assay all the samples were at the dried state, probably the conformational changes seen in SAXS and in relation to the rheological behavior observed would not be evidenced. On the other hand, the change in the temperature of the *Td* peak, which is higher for the 10% nZnO Ker thermogram could be originated in the exposure of different quantity and type of residues of the protein due to a larger interaction interface induced by the presence of nZnO agglomerates.

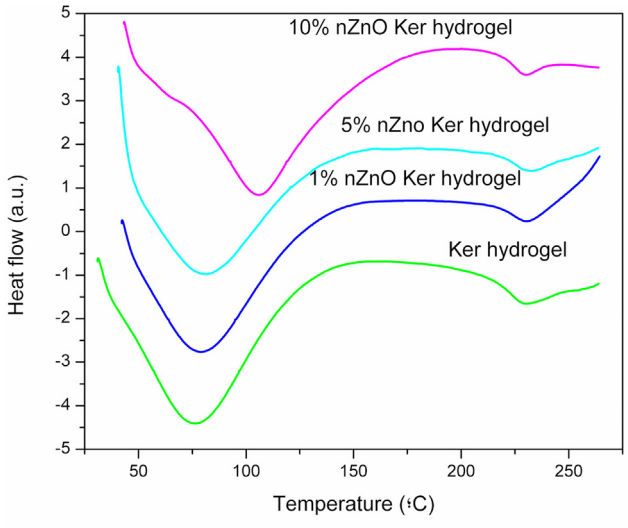

Fig. 6. DSC thermograms of the Ker and the nZnO Ker nanocomposites.

3.7. Zinc release at different pH values

The total Zinc concentration of the hydrogels was 0.63%, 3.40% and 7.28% for the ones named 1, 5 and 10% respectively. The nomenclature used for naming the different samples accounts for the original amount of nZnO used for the hydrogel synthesis. The difference in the final Zn concentration probably became for dissolution of the nanoparticles during the washing steps.

To perform this test, 10% nZnO Ker hydrogels were contacted with an agar gel equilibrated at pH 4 and pH 8 for 24 h. After that time, the amount of Zn that had been transferred to the agar was quantified. The Zn release at pH 4 was $23.4 \pm 1.9\ \mu g\ g^{-1}$ and at pH 8 it was $40.4 \pm 1.0\ \mu g\ g^{-1}$. At pH 8 the release was greater than at pH 4 ($p < 0.0001$, Student's test), suggesting that at basic pHs the pores of the hydrogel expanded allowing a greater release of nanoparticles or the Zn ion. Probably with the pore opening, the intrusion of water increased the intraparticle diffusion enhancing the mobility of the Zn^{2+} specie formed by the dissolution of the particle. This increment in the water content of the pore would lead the displacement of the nanoparticle dissolution equilibrium favoring the Zn^{2+} release.

3.8. Antimicrobial studies

The nZnO minimum inhibitory concentration was $7.8\ \mu g\ mL^{-1}$. Results (Table 1 and Fig. S4, Supplementary information) showed that those hydrogels having a concentration of 5 and 10% nZnO exhibited a good antimicrobial activity against both a Gram positive (*S. aureus*) and a Gram negative (*E. coli*) bacteria at the pH of the culture medium which is 7.0. The R(log) was above 2 in all cases, which was the value required by the JIS standard to consider a material as an effective antimicrobial. As expected, the 10% nZnO Ker hydrogel presented a better performance that the 5% nZnO Ker hydrogel. The nZnO was more effective for *S. aureus*, since 1% nZnO Ker hydrogel displayed antimicrobial activity for *S. aureus* but not in *E. coli*.

This expected result is related to the Gram-negative nature of *E. coli*, which is typically characterized by an impermeable outer cell membrane that contains endotoxins and blocks antibiotics, detergents and dyes, protecting the inner membrane and the cell wall.

Table 1
Antimicrobial efficacy assay against *S. aureus* and *E. coli* of the hydrogels loaded with different concentrations of nZnO.

% nZnO	*S. aureus*				*E. coli*			
	cfu mL^{-1}	R%	R (log)	Inhibition zone diameter	cfu mL^{-1}	R%	R (log)	Inhibition zone diameter
0	$1.8\ 10^8$	–	–	Not detected	$7.1\ 10^8$	–	–	Not detected
1	$1.0\ 10^5$	99.985	4.42	Not detected	$2.3\ 10^7$	96.812	1.94	Not detected
5	$3.3\ 10^2$	99.999	6.33	1.35 ± 0.13	$2.0\ 10^2$	99.999	6.45	0.77 ± 0.10
10	$1.66\ 10^2$	99.999	6.70	1.90 ± 0.27	$1.7\ 10^2$	99.999	6.70	0.96 ± 0.07

Table 2
Cytotoxicity evaluation.

nZnO concentration (%) Control	Viable cells (%) 100	
	Hydrogel	Extract
0	98.8 ± 4.5	97.2 ± 2.7
1	97.0 ± 2.3	96.5 ± 3.4
5	90.4 ± 3.7	87.2 ± 1.6
10	44.3 ± 5.4	32.2 ± 6.2

3.9. Cytotoxicity

The evaluation of cell cytotoxicity was performed both qualitatively and quantitatively. The qualitative assay assigned a grade of cytotoxicity from 0 to 4 according to cell damage. In this regard, qualitative evaluation a grade 2 or higher is considered a cytotoxic effect. In the case of Ker hydrogel, the degree of cytotoxicity was 0. In all cases, the results obtained by the method of direct contact of the hydrogels with the cell monolayer were in agreement with those obtained by adding the hydrogel extracts to the culture medium. In both cases of 1% and 5% nZnO Ker hydrogels exhibited a cytotoxicity of grade 1. In contrast, 10% nZnO Ker hydrogel, displayed cytotoxicity of grade 3 (Table 2). Regarding the quantitative analysis, a value <70% of viable cells was considered as cytotoxic. The results are shown in Table 2. In concordance with the qualitatively assays, the 10**%** nZnO Ker hydrogel turned out to be cytotoxic.

4. Conclusion

The aim of this work was to develop and characterize a hybrid material with keratin and Zinc Oxide nanoplates (nZnO) taking advantage of the known antimicrobial activity of nZnO and the stimuli responsive behavior of the keratin hydrogels obtained by a method develop by our previous work [12,15]. This antimicrobial hydrogel was designed for their potential use as a wound dressing, in which the biocidal agent (nZnO) will be released to a greater extent if a bacterial contamination is present. In this way, if the wound is clean, the dressing would be the barrier that isolates the injury from the environment and protects it from microbial contamination and trauma. In the presence of microorganisms and the pH change that the microbial metabolism generates, the hydrogel would swell by increasing the size of its pores and would release the biocide agent to the medium, preventing the spread of the infection.

The obtained product had a good mechanical strength and was malleable. It also had good antimicrobial activity and the release of the antimicrobial agent occurred to a greater extent at more basic pH values. The biocide effect raised along with nZnO concentration. Nevertheless, cytotoxicity also raised with nanoparticle concentration. Besides, the mechanical strength was lower due to particle agglomeration. Therefore, the optimum concentration must consider the three effects, choosing the 5% nZnO hydrogel as the best one for wound dressing applications.

The introduction of nZnO is an interesting alternative to the Ag nanoparticles, which due to the extensive use of silver ion have shown to induce antimicrobial resistance [46]. Also, nZnO could be an alternative to Cu nanoparticles which are unstable and need caping agents in order to gain stability [47]. Currently, there are different companies in the world that sell dressings with antimicrobial properties, among the most commercialized are hydrogels, hydrocolloids or sponges. In addition, the use of this type of dressings releases the biocidal agent regardless of whether an infection exists or not, exposing the patient unnecessarily. For a proper storage and application, as many other commercial hydrogels, this material could be freeze dried, sterilized by gamma irradiation, and reconstituted by hydration with the desired solution before application.

Acknowledgment

M.E.V. is grateful for her posdoctoral fellowship granted by Consejo Nacional de Investigaciones Científicas y Técnicas. The authors are grateful with Instituto Nacional de Tecnología Industrial – Mecánica (INTI) and M.Pianetti for their assistance in SEM observations. This work was supported with grants from LOréal Fundation-Unesco "For Women in science" Fellowship), Universidad de Buenos Aires (UBACYT 20020130100780BA and 13-16/021), Consejo Nacional de Investigaciones Científicas y Técnicas (PIP 10-12/PIP 076) and Agencia Nacional de Promoción Científica y Tecnológica (PICT 2012 0716, PICT-2015-0714 and PICT 2016 1997).

Appendix A. Supplementary material

Supplementary data to this article can be found online at https://doi.org/10.1016/j.jcis.2018.10.067.

References

[1] W. Paul, C.P. Sharma, Chitosan and alginate wound dressings: a short review, Trends Biomater. Artif. Organs 18 (2004) 18–23.
[2] J. Berger, M. Reist, J.M. Mayer, O. Felt, N.A. Peppas, R. Gurny, Structure and interactions in covalently and ionically crosslinked chitosan hydrogels for biomedical applications, Eur. J. Pharm. Biopharm. 57 (2004) 19–34.
[3] H. Kirsebom, M.R. Aguilar, J. San Román, M. Fernandez, M.A. Prieto, B. Bondar, Macroporous scaffolds based on chitosan and bioactive molecules, J. Bioact. Compat. Polym. 22 (2007) 621–636.
[4] H. Ueno, T. Mori, T. Fujinaga, Topical formulations and wound healing applications of chitosan, Adv. Drug Deliv. Rev. 52 (2001) 105–115.
[5] L.G. Ovington, Advances in wound dressings, Clin. Dermatol. 25 (2007) 33–38.
[6] M.-S. Kim, Y.-J. Choi, I. Noh, G. Tae, Synthesis and characterization of in situ chitosan-based hydrogel via grafting of carboxyethyl acrylate, J. Biomed. Mater. Res. A 83 (2007) 674–682.
[7] A. Hassan, M.B.K. Niazi, A. Hussain, S. Farrukh, T. Ahmad, Development of antibacterial pva/starch based hydrogel membrane for wound dressing, J. Polym. Environ. 26 (2018) 235–243.
[8] P. Gao, K. Li, Z. Liu, B. Liu, C. Ma, G. Xue, M. Zhou, Feather keratin deposits as biosorbent for the removal of methylene blue from aqueous solution: equilibrium, kinetics, and thermodynamics studies, Water. Air. Soil Pollut. 225 (2014) 1946.
[9] P. Gao, Z. Liu, X. Wu, Z. Cao, Y. Zhuang, W. Sun, G. Xue, M. Zhou, Biosorption of chromium (VI) ions by deposits produced from chicken feathers after soluble keratin extraction, CLEAN–Soil Air Water. 42 (2014) 1558–1566.
[10] P. Hill, H. Brantley, M. Van Dyke, Some properties of keratin biomaterials: kerateines, Biomaterials 31 (2010) 585–593.

[11] R.C. de Guzman, M.R. Merrill, J.R. Richter, R.I. Hamzi, O.K. Greengauz-Roberts, M.E. Van Dyke, Mechanical and biological properties of keratose biomaterials, Biomaterials 32 (2011) 8205–8217.
[12] M.L.P. Ramos, J.A. González, L. Fabian, C.J. Pérez, M.E. Villanueva, G.J. Copello, Sustainable and smart keratin hydrogel with pH-sensitive swelling and enhanced mechanical properties, Mater. Sci. Eng. C 78 (2017) 619–626.
[13] K.A.M. Amin, Reinforced materials based on chitosan, TiO_2 and Ag composites, Polymers 4 (2012) 590–599.
[14] C. Rodríguez-González, A.L. Martínez-Hernández, V.M. Castaño, O.V. Kharissova, R.S. Ruoff, C. Velasco-Santos, Polysaccharide nanocomposites reinforced with graphene oxide and keratin-grafted graphene oxide, Ind. Eng. Chem. Res. 51 (2012) 3619–3629.
[15] N. Padmavathy, R. Vijayaraghavan, Enhanced bioactivity of ZnO nanoparticles—an antimicrobial study, Sci. Technol. Adv. Mater. (2016).
[16] C. Wang, L.-L. Liu, A.-T. Zhang, P. Xie, J.-J. Lu, X.-T. Zou, Antibacterial effects of zinc oxide nanoparticles on Escherichia coli K88, Afr. J. Biotechnol. 11 (2016) 10248–10254.
[17] P.T. Kumar, V.-K. Lakshmanan, R. Biswas, S.V. Nair, R. Jayakumar, Synthesis and biological evaluation of chitin hydrogel/nano ZnO composite bandage as antibacterial wound dressing, J. Biomed. Nanotechnol. 8 (2012) 891–900.
[18] K.T. Shalumon, K.H. Anulekha, S.V. Nair, S.V. Nair, K.P. Chennazhi, R. Jayakumar, Sodium alginate/poly (vinyl alcohol)/nano ZnO composite nanofibers for antibacterial wound dressings, Int. J. Biol. Macromol. 49 (2011) 247–254.
[19] P.T. Sudheesh Kumar, V.-K. Lakshmanan, T.V. Anilkumar, C. Ramya, P. Reshmi, A.G. Unnikrishnan, S.V. Nair, R. Jayakumar, Flexible and microporous chitosan hydrogel/nano ZnO composite bandages for wound dressing: in vitro and in vivo evaluation, ACS Appl. Mater. Interf. 4 (2012) 2618–2629.
[20] S. Nair, A. Sasidharan, V.D. Rani, D. Menon, S. Nair, K. Manzoor, S. Raina, Role of size scale of ZnO nanoparticles and microparticles on toxicity toward bacteria and osteoblast cancer cells, J. Mater. Sci. Mater. Med. 20 (2009) 235–241.
[21] P.J.P. Espitia, N.deF.F. Soares, J.S. dos Reis Coimbra, N.J. de Andrade, R.S. Cruz, E. A.A. Medeiros, Zinc oxide nanoparticles: synthesis, antimicrobial activity and food packaging applications, Food Bioprocess Technol. 5 (2012) 1447–1464.
[22] R. Dutta, B.P. Nenavathu, M.K. Gangishetty, A. Reddy, Studies on antibacterial activity of ZnO nanoparticles by ROS induced lipid peroxidation, Colloids Surf. B Biointerf. 94 (2012) 143–150.
[23] A. Sasidharan, P. Chandran, D. Menon, S. Raman, S. Nair, M. Koyakutty, Rapid dissolution of ZnO nanocrystals in acidic cancer microenvironment leading to preferential apoptosis, Nanoscale 3 (2011) 3657–3669.
[24] A. Becheri, M. Dürr, P.L. Nostro, P. Baglioni, Synthesis and characterization of zinc oxide nanoparticles: application to textiles as UV-absorbers, J. Nanoparticle Res. 10 (2008) 679–689.
[25] R. Jalal, E.K. Goharshadi, M. Abareshi, M. Moosavi, A. Yousefi, P. Nancarrow, ZnO nanofluids: green synthesis, characterization, and antibacterial activity, Mater. Chem. Phys. 121 (2010) 198–201.
[26] R. Jayakumar, M. Prabaharan, P.S. Kumar, S.V. Nair, H. Tamura, Biomaterials based on chitin and chitosan in wound dressing applications, Biotechnol. Adv. 29 (2011) 322–337.
[27] L.A. Schneider, A. Korber, S. Grabbe, J. Dissemond, Influence of pH on wound-healing: a new perspective for wound-therapy?, Arch Dermatol. Res. 298 (2007) 413–420.
[28] G. Gethin, The significance of surface pH in chronic wounds, Wounds UK 3 (2007) 52.
[29] Japanese Industrial Standard (JIS) Z 2801, (n.d.).
[30] V. Gadenne, L. Lebrun, T. Jouenne, P. Thebault, Antiadhesive activity of ulvan polysaccharides covalently immobilized onto titanium surface, Colloids Surf. B Biointerf. 112 (2013) 229–236.
[31] M. Pollini, F. Paladini, A. Licciulli, A. Maffezzoli, L. Nicolais, A. Sannino, Silver-coated wool yarns with durable antibacterial properties, J. Appl. Polym. Sci. 125 (2012) 2239–2244.
[32] UNE-EN ISO 10993-5:2009 Evaluación biológica de productos sanitarios. Parte 5: Ensayos de citotoxicidad in vitro (ISO 10993-5:2009), (n.d.).
[33] M. Bitenc, G. Dražić, Z.C. Orel, Characterization of crystalline zinc oxide in the form of hexagonal bipods, Cryst. Growth Des. 10 (2010) 830–837, https://doi.org/10.1021/cg901193g.
[34] K. Kakiuchi, E. Hosono, T. Kimura, H. Imai, S. Fujihara, Fabrication of mesoporous ZnO nanosheets from precursor templates grown in aqueous solutions, J. Sol-Gel Sci. Technol. 39 (2006) 63–72.
[35] M. Park, B.-S. Kim, H.K. Shin, S.-J. Park, H.-Y. Kim, Preparation and characterization of keratin-based biocomposite hydrogels prepared by electron beam irradiation, Mater. Sci. Eng. C. 33 (2013) 5051–5057, https://doi.org/10.1016/j.msec.2013.08.032.
[36] P. Kakkar, B. Madhan, G. Shanmugam, Extraction and characterization of keratin from bovine hoof: a potential material for biomedical applications, SpringerPlus 3 (2014) 596.
[37] S. Wang, F. Taraballi, L.P. Tan, K.W. Ng, Human keratin hydrogels support fibroblast attachment and proliferation in vitro, Cell Tissue Res. 347 (2012) 795–802.
[38] E. Manikandan, G. Kavitha, J. Kennedy, Epitaxial zinc oxide, graphene oxide composite thin-films by laser technique for micro-Raman and enhanced field emission study, Ceram. Int. 40 (2014) 16065–16070, https://doi.org/10.1016/j.ceramint.2014.07.129.
[39] C.J. Raj, R.K. Joshi, K.B.R. Varma, Synthesis from zinc oxalate, growth mechanism and optical properties of ZnO nano/micro structures, Cryst. Res. Technol. 46 (2011) 1181–1188, https://doi.org/10.1002/crat.201100201.
[40] Q. Xu, Z. Zhang, R. Hong, X. Chen, F. Zhang, Z. Wu, ZnO nano-platelets by laser induced plasma assisted-irradiation with a pulse KrF laser, Mater. Lett. 105 (2013) 206–208, https://doi.org/10.1016/j.matlet.2013.04.011.
[41] J. Shao, J. Zheng, J. Liu, C.M. Carr, Fourier transform Raman and Fourier transform infrared spectroscopy studies of silk fibroin, J. Appl. Polym. Sci. 96 (2005) 1999–2004, https://doi.org/10.1002/app.21346.
[42] M. Koenig, T. Kasputis, D. Schmidt, K.B. Rodenhausen, K.-J. Eichhorn, A.K. Pannier, M. Schubert, M. Stamm, P. Uhlmann, Combined QCM-D/GE as a tool to characterize stimuli-responsive swelling of and protein adsorption on polymer brushes grafted onto 3D-nanostructures, Anal. Bioanal. Chem. 406 (2014) 7233–7242.
[43] J.D. Ferry, Viscoelastic Properties of Polymers, 3rd ed., John Wiley & Sons, 1980.
[44] J. Yang, C.-R. Han, J.-F. Duan, F. Xu, R.-C. Sun, Mechanical and viscoelastic properties of cellulose nanocrystals reinforced poly(ethylene glycol) nanocomposite hydrogels, ACS Appl. Mater. Interf. 5 (2013) 3199–3207, https://doi.org/10.1021/am4001997.
[45] D. Istrate, M.E. Rafik, C. Popescu, D.E. Demco, L. Tsarkova, F.-J. Wortmann, Keratin made micro-tubes: the paradoxical thermal behavior of cortex and cuticle, Int. J. Biol. Macromol. 89 (2016) 592–598.
[46] A. Panáček, L. Kvítek, M. Smékalová, R. Večeřová, M. Kolář, M. Röderová, F. Dyčka, M. Šebela, R. Prucek, O. Tomanec, R. Zbořil, Bacterial resistance to silver nanoparticles and how to overcome it, Nat. Nanotechnol. 13 (2018) 65.
[47] M. Villanueva, A. Diez, J. Gonzalez, C. Perez, M. Orego, L. Piehl, S. Teves, G. Copello, Antimicrobial activity of starch hydrogel incorporated with copper nanoparticles, ACS Appl. Mater. Interf. 8 (25) (2016) 16280–16288.